Progress In Electromagnetics Research, Vol. 124, 347–364, 2012

ANALYSIS OF ELECTROMAGNETIC BEHAVIOR IN SWITCHED RELUCTANCE MOTOR FOR THE APPLICATION OF INTEGRATED AIR CONDITIONER ON-BOARD CHARGER SYSTEM

J. Liang[1], L. Jian[1], G. Xu[1], and Z. Shao[2,*]

[1]Shenzhen Institutes of Advanced Technology, Chinese Academy of Sciences & Chinese University of Hong Kong, 1068 Xueyuan Avenue, University Town, Shenzhen, China

[2]Department of Electrical and Electronic Engineering, The University of Hong Kong, Pokfulam Road, Hong Kong, China

Abstract—In order to achieve low cost and compact design, it becomes more and more popular to integrate the circuit of the on-board charger into other power electronic circuits existing in EVs. In this paper an integrated air conditioner on-board charger system based on switched reluctance motor (SRM) was proposed, and the electromagnetic behavior occurring in the SRM when working in the charging mode was investigated. Three charging patterns, viz. single-phase charging, double-phase charging and triple-phase charging were analyzed. The specific rotor positions for which the rotor can be kept still when injecting charging currents to the armature windings were identified. The optimal design for maximizing the keeping-still capability was conducted. The power losses occurring in the SRM when working in charging mode were estimated.

1. INTRODUCTION

Transport electrification has been considered as one of the most promising solution to the urgent challenges facing our human beings, such as global warming, environmental pollution, energy crisis and so forth [1]. Most recently, with the advent of the vehicle-to-grid (V2G) technology [2], the gridable EVs that can be directly connected to the utility grid have been expected to function as distributed energy storage system during the parking period, so as to balance the demand

Received 25 November 2011, Accepted 23 January 2012, Scheduled 2 February 2012

* Corresponding author: Ziyun Shao (zyshao@eee.hku.hk).

and supply of the electricity market in the future. Generally, gridable EVs include battery EVs, plug-in hybrid EVs [3, 4] and range-extended EVs [5].

In contrary to the traditional EVs, the gridable EVs are equipped with plugs and on-board chargers. By connecting the plug to the utility grid, the electrical energy can flow into the on-board batteries through the on-board charger. Moreover, the energy deposited in EVs can also be fed back to power grid when bi-directional on-board charger is engaged. Generally, there are two types of on-board chargers: isolated type and non-isolated type. In the isolated type, a transformer is engaged to isolate the primary side from the secondary side. While in the non-isolated type, the primary side and secondary side share the same ground, such as the charger based on boost converter. In order to reduce the overall weight and volume, it becomes more and more popular to integrate the circuit of the charger into other power electronic circuits existing in EVs. In the previous publications, the EV motor drive circuits and the AC drive motor are involved to construct integrated on-board chargers [6, 7]. Due to the neutral point of AC motors, one terminal of AC line can be conveniently connected to the neutral point, and the three-phase windings can function as the couple inductances in the boost converter circuit. However, the boost converter topology requires the input voltage lower than the output voltage. Thus, such kind of integrated charger is more feasible in countries and regions where 110 V AC power is adopted. In order to extend the range of the input voltage, the buck converter has been added to the battery side.

In addition to the three-phase AC motors, switched reluctance motor (SRM) has attracted increasing attention recently, due to its low cost, simple structure, good controllability, high efficiency and wide operation range [8–10]. SRMs have been extensively applied to the electric air conditioning systems of EVs. The purpose of this paper is to propose an integrated charger based on SRM electric air conditioner. It has two working modes: the driving mode and the charging mode. In the driving mode, the integrated system operates as an asymmetric converter to drive the SRM, thereby the compressor of the air conditioner. In the charging mode, all phase windings of the SRM are employed as inductances to achieve battery charging. Buck-boost circuit is adopted in order to satisfy the charging characteristic and power quality requirement. This paper will be focused on investigating the electromagnetic behavior occurring in the SRM when the integrated air conditioner on-board charger system working in the charging mode. Firstly, the integrated system is introduced in Section 2. Secondly, the electromagnetic characteristics

are analyzed when single-phase charging, double-phase charging and triple-phase charging are adopted, respectively. Thirdly, the optimal design of SRM for maximizing the attraction force that keeps the rotor standstill is conducted in Section 4. Fourthly, the iron losses and copper losses in SRM when injecting sinusoidal charging currents into armature windings are estimated in Section 5. Finite element method (FEM) which has been successfully used to design and analyze electromagnetic devices [11–18] will be engaged in this paper.

2. INTEGRATED SRM AIR-CONDITIONER ON-BOARD CHARGER SYSTEM

Traction battery system is one of the most critical components for EVs, especially for gridable EVs. While, the lifetime and the charging time

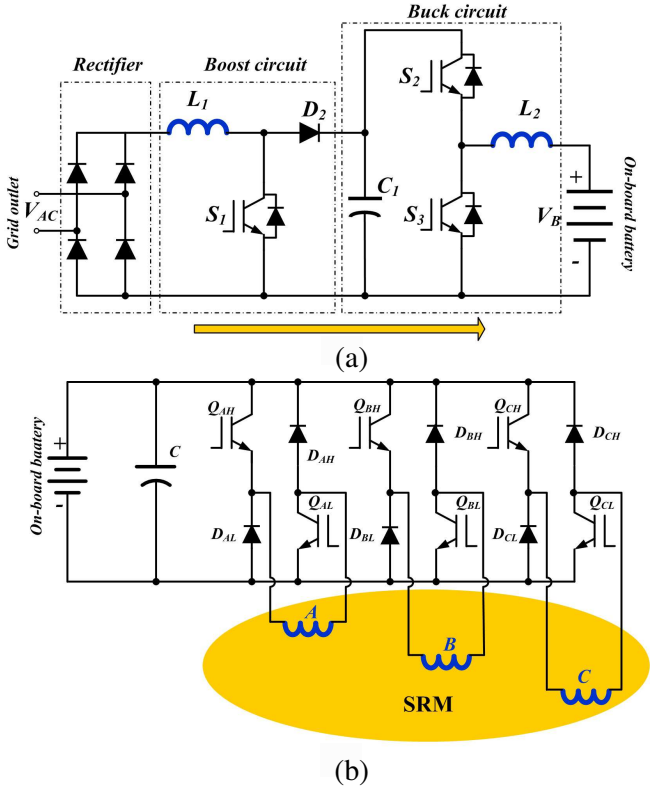

Figure 1. (a) Non-isolated on-board charger. (b) Three-phase SRM drive system.

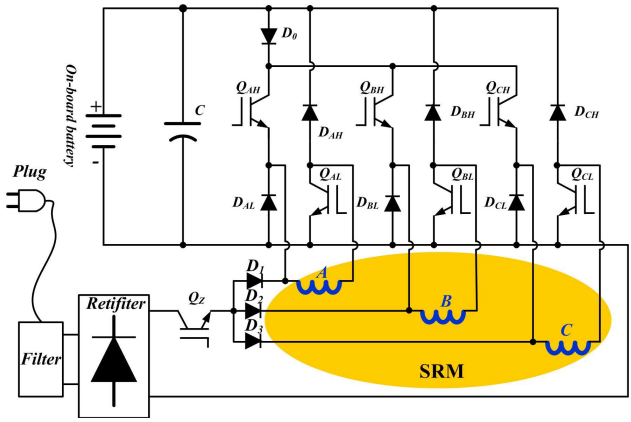

Figure 2. Integrated air-conditioner on-board charger system.

of traction batteries are strongly dependent on the characteristic of battery charger. Fig. 1(a) shows the circuit of a typical non-isolated electric vehicle charger. A boost converter is used to step up the voltage of capacitor C_1 and conduct power factor correction (PFC). Moreover, a buck converter is engaged to control the charging current, so as to satisfy the characteristic of battery. Fig. 1(b) illustrates the three-phase SRM drive system powered by the on-board batteries. A large capacitor is employed in the front-end as a low-pass filter, so as to keep a steady DC-link voltage as well as store the magnetic field energy when the SRM is demagnetized. Due to the various merits of switched reluctance motors, the SRM drive system has been extensively applied to the electric air conditioning systems of EVs.

In order to achieve compact design, an integrated air-conditioner on-board charger system is proposed as shown in Fig. 2. It can be observed that this system consists of a line filer, a rectifier, a modified asymmetric converter and some external devices. The proposed system can offer two functions: driving compressor and charging battery. For driving compressor, the power switch Q_Z is kept turned off, and the system can offer three operation modes: excitation mode, free-wheeling mode, and demagnetization mode. The energy deposited in the on-board batteries is transmitted to the SRM via the three-phase drive circuit. For charging battery, the armature windings of the SRM serves as the inductances in the buck-boost converter, and sinusoidal charging currents flow from the outlet of the utility grid to the on-board batteries.

In order to improve the overall efficiency, the rotor of the SRM should be kept still when injecting the charging currents to its

windings. Two ways can be selected: mechanical brake method and zero torque control method. For the mechanical brake method, additional mechanical mechanism should be used to lock the rotor. With no doubt, this will increase the cost of the system. For the zero torque control method, special rotor positions are chosen in order to make the electromagnetic torque of SRM to be zero when injecting sinusoidal charging current. Moreover, according to the demand of charging power, three kinds of the charging modes can be executed, which includes the single-phase-charging mode, the double-phase-charging mode and the triple-phase-charging mode, respectively.

3. ELECTROMAGNETIC PERFORMANCE OF SRM WHEN INJECTING CHARGING CURRENTS

3.1. Traction Force in SRM

The topology of the SRM investigated in this paper is illustrated in Fig. 3(a). It has 8 rotor poles and 12 stator poles. The three-phase windings are wounded on the stator poles, and there are four coils for each phase. Table 1 gives the specifications of the SRM investigated in this paper. Fig. 3(b) can help figure out how the attraction force is produced between one stator pole and one rotor pole. It is easy to know that the electromagnetic flux lines will pass through the overlapped area due to fringing effect, and the inductance can be modeled as:

$$L = \frac{\mu_0 N^2 L_{\text{stk}} R}{g}(\theta_0 + K_f) \tag{1}$$

where μ_0 is the permeability of the air space, K_f is a constant for the fringing inductance, N is the number of coil turns, L_{stk} is the motor stacking length, R is the rotor radius, g is the air gap length, θ_0 is the overlapping angle, respectively. Let the amplitude and angle of the attraction force for the pole be F and θ_F, respectively. According to (1), F can be approximated as:

$$F = K_F i^2 \tag{2}$$

in which $K_F = L/4g$.

In what follows, the specific positions where the overall electromagnetic torque exerted on the rotor is equal to zero when injecting charging currents into the armature windings will be investigated, so as to improve the charging efficiency of the system. In addition, the optimal design of SRM for increasing its keeping-still ability will be conducted. The rotor tooth β_r shown in Fig. 3(b) is the main factor to be considered.

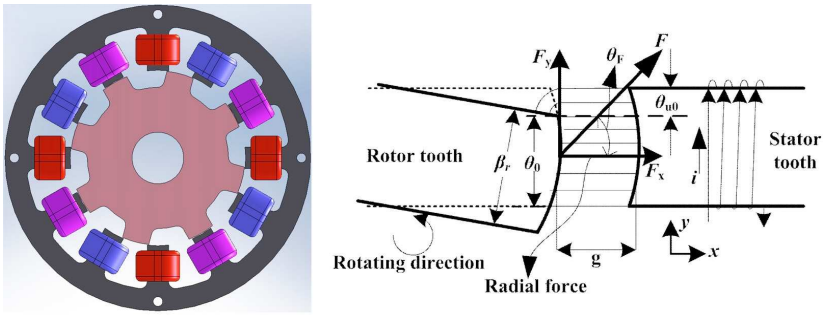

Figure 3. (a) Topology of SRM investigated. (b) Attraction force produced between one stator pole and one rotor pole.

Table 1. Specifications of SRM Investigated.

Number of stator poles	12
Number of rotor poles	8
Pole arc of stator	15 Degree
Pole arc of rotor	16 Degree
Outer diameter of stator	132 mm
Inner diameter of stator	73 mm
Yoke thickness of stator	9.5 mm
Yoke thickness of rotor	6.5 mm
Phase resistance	1 Ω
Number of turns per coil	120
Length of airgap	0.3 mm

3.2. Electromagnetic Performance with Single-phase Charging

When the demanded charging power is low, such as in the cases of overnight charging, single-phase charging could be employed. As shown in Figs. 4(a) and (b), it can be known that there are two specific rotor positions where the overall electromagnetic torque could be zero when injecting the charging current into phase-A, one is at the position of 0 Degree and the other is at the position of 22.5 Degree. The corresponding electromagnetic flux distributions obtained by using FEM are illustrated in Figs. 4(c) and (d). The number of elements in the mesh is 40194. The charging power is 500 W, and the

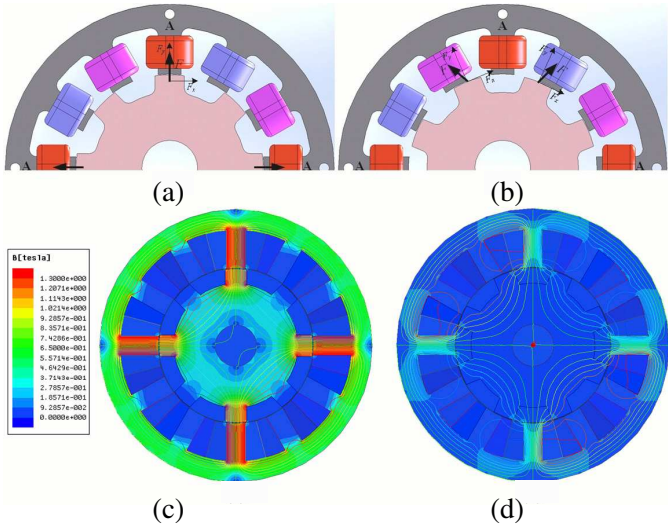

Figure 4. Zero-torque positions and flux distributions with single-phase charging. (a) Zero-torque position: 0 Degree. (b) Zero-torque position: 22.5 Degree. (c) Flux distribution at 0 Degree. (d) Flux distribution at 22.5 Degree.

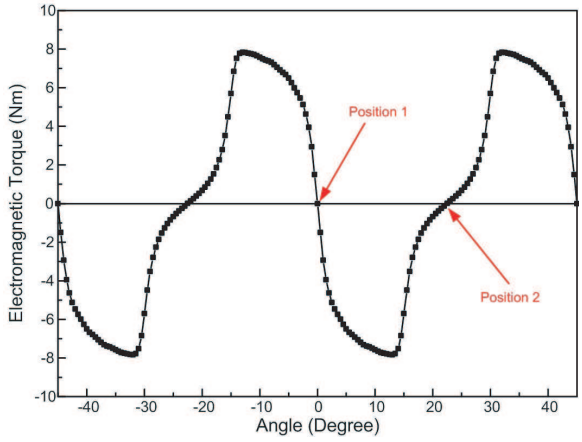

Figure 5. Electromagnetic torque versus rotor position when injecting charging current to phase-A.

charging current is 3.5 Arms. It can be observed that the flux lines are distributed symmetrically in the iron yokes, and this implies the balance of traction forces has been reached. However, this does not mean that both rotor positions are suitable for single-phase charging.

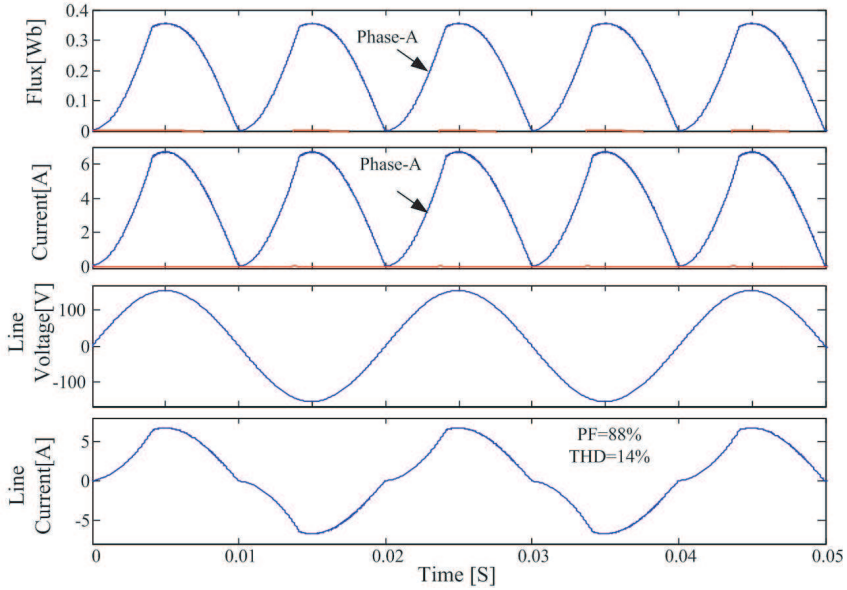

Figure 6. Charging waveforms in single-phase charging process.

Fig. 5 gives the calculated electromagnetic torques at different rotor positions when injecting the charging current into phase-A by using FEM. It can be observed that the derivative of the torque-angle curves at the position of 0 Degree is negative. This means that if the rotor is aligned at the position of 0 Degree, and some disturbances happen to make the rotor to drift off the original position, the produced electromagnetic torque will force it back to the original position. In other words, the position of 0 Degree is a stable point for the rotor when single-phase charging (phase-A) is being conducted. Nevertheless, the derivative of the torque-angle curves at the position of 22.5 Degree is positive. This means that the rotor will be dragged even far away from the original position by the produced electromagnetic torque when disturbance occurs. Thus, the position of 22.5 Degree is an unstable balance point, and it is not suitable for single-phase charging. Fig. 6 shows the charging waveforms in single-phase charging process calculated by using FEM.

3.3. Electromagnetic Performance with Double-phase Charging

When higher charging power is demanded, the double-phase charging could be adopted. As shown in Figs. 7(a) and (b), it can be known

that there are also two specific rotor positions where the overall electromagnetic torque could be zero when injecting the charging current into both phase-A and phase-B, one is at the position of 7.5 Degree and the other is at the position of 30 Degree. Assuming the

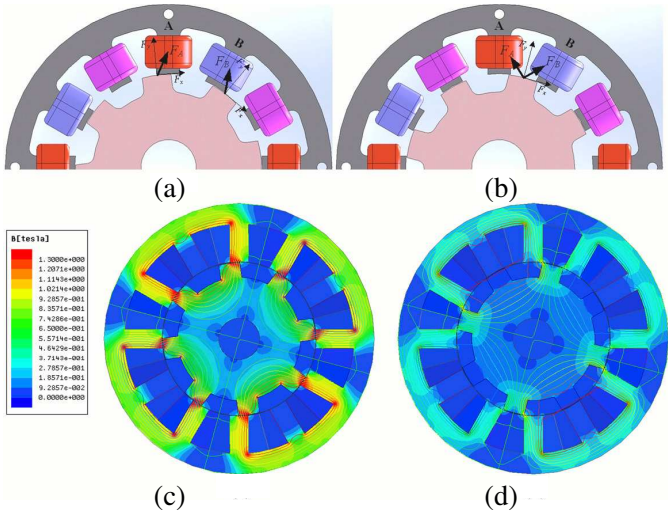

Figure 7. Zero-torque positions and flux distributions with double-phase charging. (a) Zero-torque position: 7.5 Degree. (b) Zero-torque position: 30 Degree. (c) Flux distribution at 7.5 Degree. (d) Flux distribution at 30 Degree.

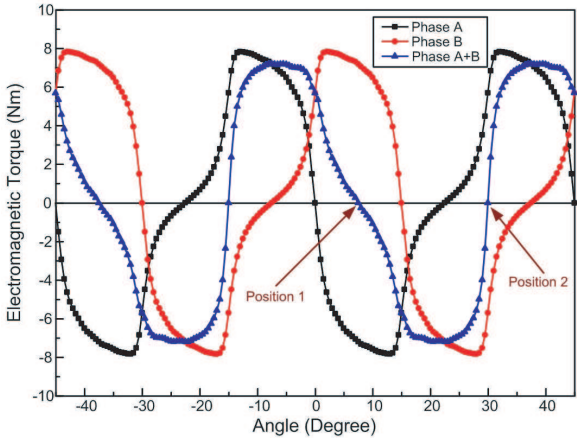

Figure 8. Electromagnetic torque versus rotor position when injecting charging current to phase-A and phase-B.

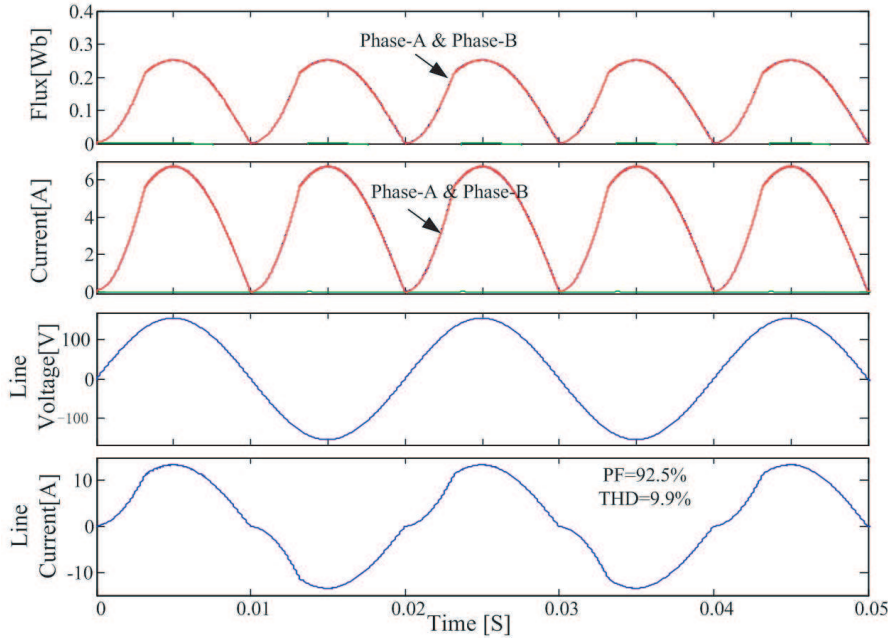

Figure 9. Charging waveforms in double-phase charging process.

charging power is 1 kW, phase-A and phase-B take 500 W each, and the charging current in each phase is equal to 3.5 Arms. The corresponding electromagnetic flux distributions are illustrated in Figs. 7(c) and (d). Fig. 8 gives the calculated electromagnetic torques at different rotor positions when injecting the charging current into phase-A and phase-B by using FEM. It can be observed that the derivative of the torque-angle curves at the position of 7.5 Degree is negative, while that at the position of 30 degree is positive. For the same reason presented in the above section, it can be known that the position of 30 Degree is an unstable balance point, and it is not suitable for double-phase charging. Fig. 9 shows the charging waveforms in double-phase charging process calculated by using FEM.

3.4. Electromagnetic Performance with Triple-phase Charging

When triple-phase charging is engaged, the phase A, B and C can bear equivalent charging power, and the specific rotor positions where the overall electromagnetic torque could be zero when injecting equivalent charging currents into the three phases are indicated in Fig. 10. There

are six positions: Position 1 (angle of 0 Degree), Position 2 (angle of 7.5 Degree), Position 3 (angle of 15 Degree), Position 4 (angle of 22.5 Degree), Position 5 (angle of 30 Degree) and Position 6 (angle of 37.5 Degree). Assuming the charging power is 1.5 kW, phase-A, phase-B and phase-C take 500 W each, and the charging current in each phase is equal to 3.5 Arms, the flux distributions at the specific positions are illustrated in Fig. 11. Fig. 12 gives the calculated electromagnetic torque. It can be found that only the Positions 2, 4 and 6 are stable balance points for triple-phase equivalent charging. Compared with the case of single-phase charging (as shown in Fig. 6) and the case of double-phase charging (as shown in Fig. 9), it can also be found that in the case of triple-phase equivalent charging, the slopes of the torque-angle curves at the stable balance points are quite small. This means that the capability for keeping the rotor still when is very weak when equivalent triple-phase charging is employed. For this reason, we investigated the performance of triple-phase nonequivalent charging. Fig. 13 gives the calculated torque-angle curves of three triple-phase nonequivalent charging cases. In case 1, the phase A takes 500 W, phase B and C take 50 W each. In case 2, the phase A takes 500 W,

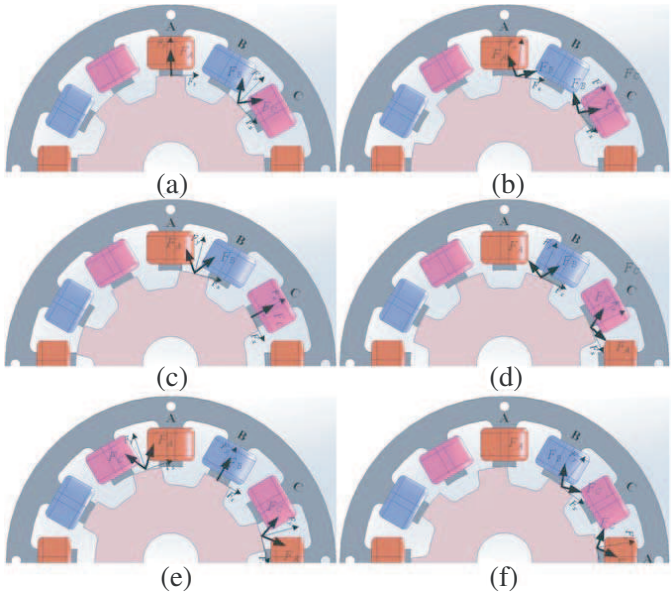

Figure 10. Zero-torque positions with triple-phase charging. (a) Rotor at position of 0 Degree. (b) Rotor at position of 7.5 Degree. (c) Rotor at position of 15 Degree. (d) Rotor at position of 22.5 Degree. (e) Rotor at position of 30 Degree. (f) Rotor at position of 37.5 Degree.

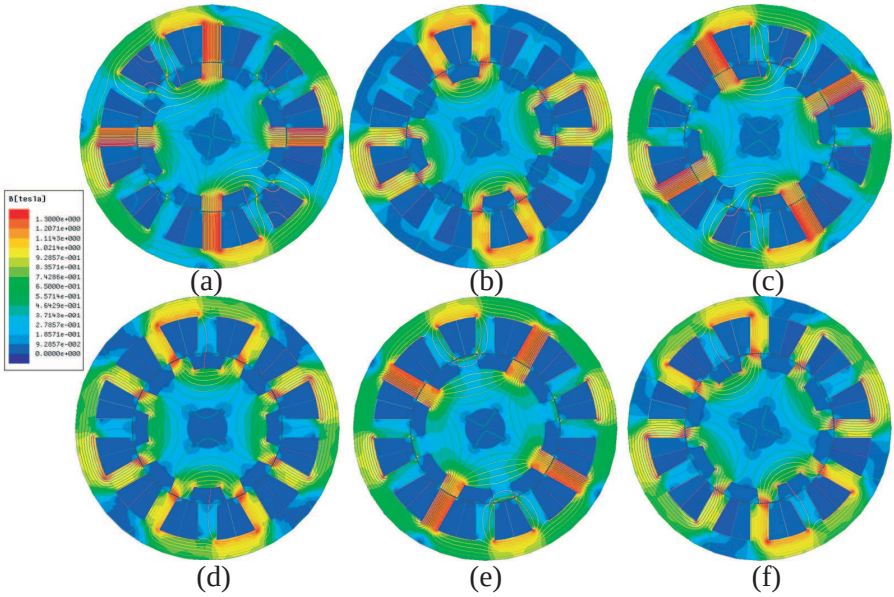

Figure 11. Flux distribution with triple-phase equivalent charging. (a) Rotor at position of 0 Degree. (b) Rotor at position of 7.5 Degree. (c) Rotor at position of 15 Degree. (d) Rotor at position of 22.5 Degree. (e) Rotor at position of 30 Degree. (f) Rotor at position of 37.5 Degree.

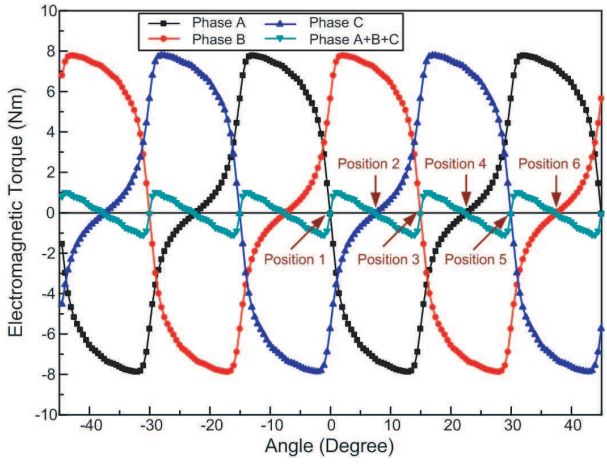

Figure 12. Electromagnetic torque versus rotor position when injecting equivalent charging current to phase-A, phase-B and phase-C.

phase B and C take 200 W each. In case 3, the phase A takes 500 W, phase B and C take 350 W each. It can be observed that, in these three cases, the stable balance charging point turns into the angle of 0 Degree. Moreover, their stability is much stronger than that of the triple-phase equivalent charging.

So far, three charging modes, including the single-phase charging, the double-phase charging and the triple-phase charging have been investigated. The charging mode adopted could be chosen according to the required charging power. Fig. 15(a) shows one of the mode selection strategy: if the require charging power is less than or equal to 500 W, the single phase charging (Phase-A, for example) is selected; if the power is in between 500 W and 1000 W, the double phase charging (Phase-A and -B, for example) is selected; otherwise if the power is in between 1000 W and 1500 W, the triple phase charging is selected. The biggest problem of this selection strategy is that the rotor position should be changed when the charging mode changes. Fig. 15(b) shows another mode selection strategy: if the required charging power is less than or equal to 500 W, the single phase charging (Phase-A, for example) is selected; otherwise, if the required power is bigger than 500 W, both other two phases (Phase-B and -C, for example) should be employed to take the extra power equally. According to Fig. 5 and Fig. 13, it can be understood that the rotor always stays at the position of 0 Degree. However, the maximum power taken by using this strategy is about 1.2 kW.

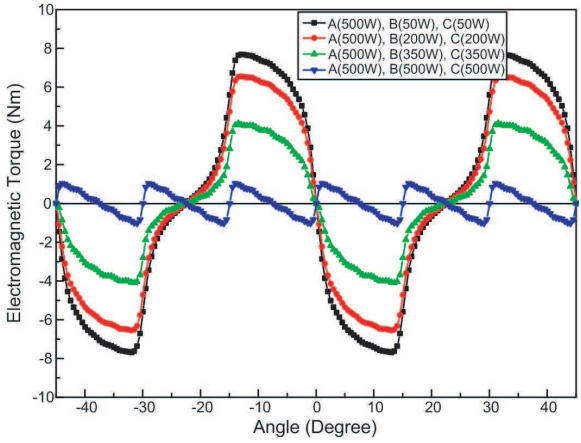

Figure 13. Electromagnetic torque versus rotor position when injecting nonequivalent charging current to phase-A, phase-B and phase-C.

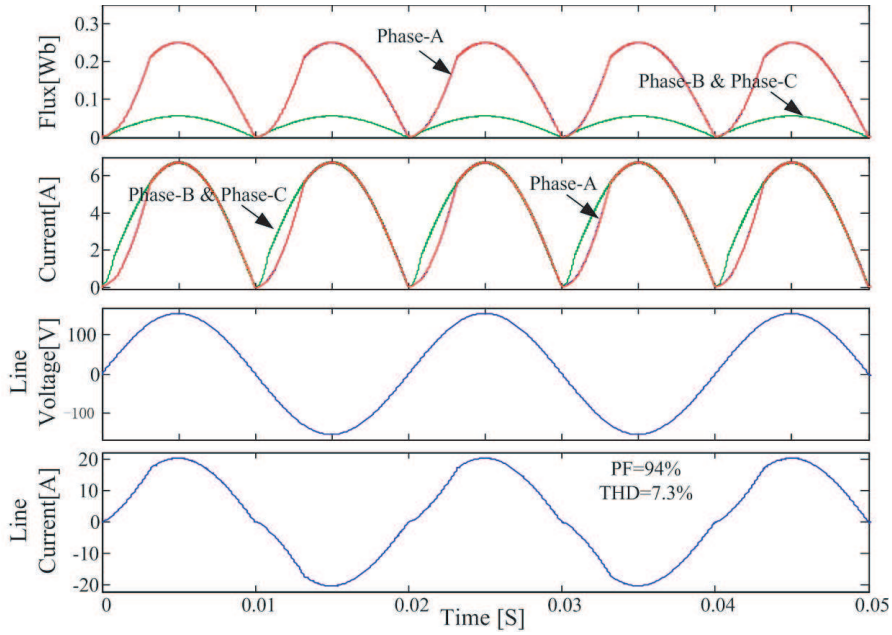

Figure 14. Charging waveforms in triple-phase charging process.

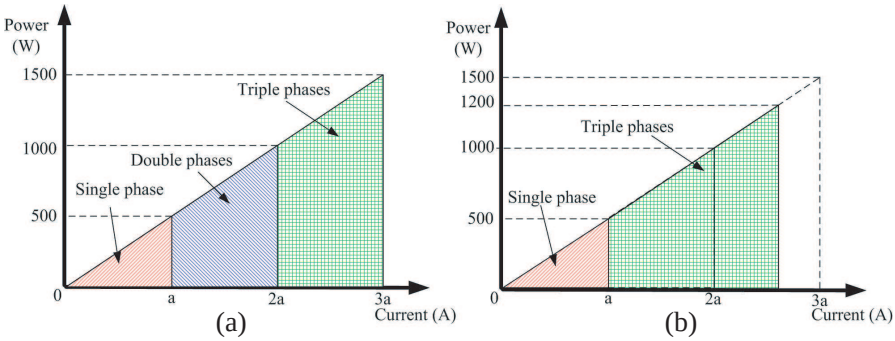

Figure 15. Charging mode selection strategy. (a) Three modes charging. (b) Two modes charging.

4. OPTIMAL DESIGN FOR IMPROVING THE KEEPING STILL CAPABILITY

As aforementioned, it is quite important to keep the rotor still when charging the batteries. Otherwise, the vibration or the rotation of the rotor will cause the uncertain of the armature inductance, and this

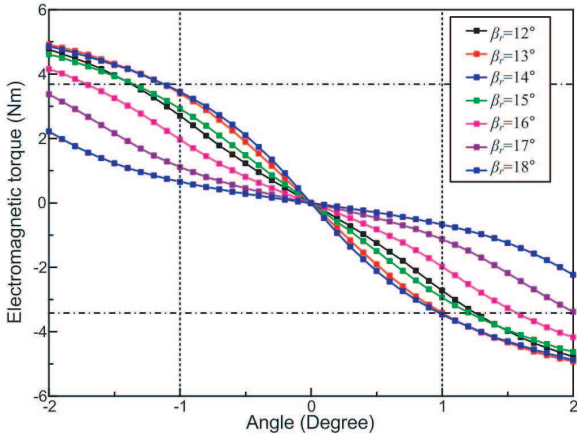

Figure 16. Electromagnetic torque with different rotor pole width angle when single-phase charging is conducted.

may make the power electronic circuit fail to function. In addition, the moving of the rotor will arouse several nuisances, such as power loss, audible noise and mechanical vibration. Actually, the keeping still capability can be improved by the optimal design of the rotor pole shape. For the considered SRM, there are 12 stator poles and 8 rotor poles, and the width angle of the stator pole equals 15 Degree. Fig. 16 illustrates the developed electromagnetic torque with different width angle of the rotor pole when single-phase charging is conducted. It can be observed that if we assume the rotor rotates 1 Degree away from the balance point, the electromagnetic torque that will force it back is strongly depended on the width angle of the rotor pole. The smallest torque value is about 0.9 Nm in the case of β_r equal to 18 Degree, while, the biggest torque value is about 3.6 Nm in the case of β_r equal to 14 Degree. Generally, the optimal rotor pole width angle should be close to the stator pole width angle, but it can not be exactly equal to that.

5. POWER LOSSES ANALYSIS

The power losses consist of the core loss occurring in the iron yokes and the copper loss occurring in the armature windings. The core loss which is composed of the eddy current loss and the hysteresis loss can be predicted by using FEM. Fig. 17 illustrates the calculated core loss with different charging patterns. The frequency of the charging currents is 50 Hz. After about 15 ms, the electromagnetic process enters

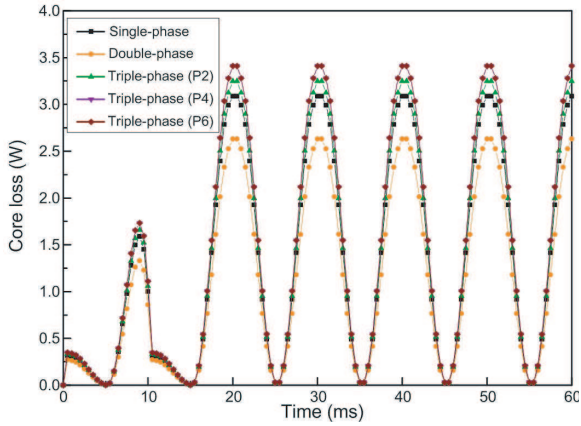

Figure 17. Core losses with different charging patterns.

Table 2. Power losses with different charging patterns.

Charging Pattern	Core Losses	Copper Losses	Pout	Efficiency
Single-Phase	1.622 W	22.5 W	500 W	95.176%
Double-Phase	1.365 W	45.0 W	1000 W	95.363%
Triple-Phase(P2)	1.693 W	67.5 W	1500 W	95.387%
Triple-Phase(P4)	1.782 W	67.5 W	1500 W	95.381%
Triple-Phase(P6)	1.782 W	67.5 W	1500 W	95.381%

the stable stage. The core loss in triple-phase charging is slightly larger than that in double-phase charging, and also the single-phase charging. For the triple-phase charging, the core loss when rotor in Position 4 and Position 6 are the same with each other, and bigger than the core loss when rotor in Position 2. Table 2 lists the details on the power losses and the resulted charging efficiency. Compared with the copper losses, the core losses are rather trivial, and almost can be ignored. The efficiency is higher than 95 %, and this is quite acceptable for on board battery charging.

6. CONCLUSION

In this paper, an integrated air conditioner on-board charger system was proposed, and the electromagnetic behavior occurring in the SRM when working in the charging mode was investigated. Firstly, three charging patterns, viz. single-phase charging, double-phase charging

and triple-phase charging were analyzed. The specific rotor positions for which the rotor can be kept still when injecting charging currents to the armature windings were identified. Secondly, the keeping-still capability can be improved by adjusting the width angle of the rotor pole. Generally, the optimal rotor pole width angle should be close to the stator pole width angle, but it can not be exactly equal to that. Finally, the power losses occurring in the SRM when working in charging mode was estimated. The FEM results demonstrate that the efficiency can be over 95%, which is quite acceptable for on board charging.

REFERENCES

1. Chan, C. C., "The state of the art of electric, hybrid, and fuel cell vehicles," *Proceeding of the IEEE*, Vol. 95, No. 4, 704–718, 2007.
2. Dyke, K. J., N. Schofield, and M. Barnes, "The impact of transport electrification on electrical networks," *IEEE Trans. Ind. Electron.*, Vol. 57, No. 12, 3917–3926, 2010.
3. Mapelli, F. L., D. Tarsitano, and M. Mauri, "Plug-in hybrid electric vehicle: modeling, prototype, realization, and inverter losses reduction analysis," *IEEE Trans. Ind. Electron.*, Vol. 57, No. 2, 598–607, 2010.
4. Saber, A. Y. and G. K. Venayagamoorthy, "Plug-in vehicles and renewable energy sources for cost and emission reductions," *IEEE Trans. Ind. Electron.*, Vol. 58, No. 4, 1229–1238, 2011.
5. Wieringen, V. and R. Pop-Iliev, "Development of a dual-fuel power generation system for an extended range plug-in hybrid electric vehicle," *IEEE Trans. Ind. Electron.*, Vol. 57, No. 2, 641–648, 2010.
6. Sul, S. K. and S. J. Lee, "An integral battery charger for four-wheel drive electric vehicle," *IEEE Trans. Ind. Appl.*, Vol. 31, No. 5, 1096–1099, 1995.
7. Pellegrino, G., E. Armando, and P. Guglielmi, "An integral battery charger with power factor correction for electric scooter," *IEEE Trans. Pow. Electron.*, Vol. 25, No. 3, 751–759, 2010.
8. Torkaman, H. and E. Afjei, "FEM analysis of angular misalignment fault in SRM magnetostatic characteristics," *Progress In Electromagnetics Research*, Vol. 104, 31–48, 2010.
9. Torkaman, H. and E. Afjei, "Hybrid method of obtaining degrees of freedom for radial airgap length in SRM under normal and faulty conditions based on magnetostatic model," *Progress In Electromagnetics Research*, Vol. 100, 37–54, 2010.

10. Zhao, W., M. Cheng, R. Cao, and J. Ji, "Experimental comparison of remedial single-channel operations for redundant flux-switching permanent-magnet motor drive," *Progress In Electromagnetics Research*, Vol. 123, 189–204, 2012.
11. Jian, L., G. Xu, Y. Gong, J. Song, J. Liang, and M. Chang, "Electromagnetic design and analysis of a novel magnetic-gear-integrated wind power generator using time-stepping finite element method," *Progress In Electromagnetics Research*, Vol. 113, 351–367, 2011.
12. Jian, L. and K. T. Chau, "Design and analysis of a magnetic-geared electronic-continuously variable transmission system using finite element method," *Progress In Electromagnetics Research*, Vol. 107, 47–61, 2010.
13. Faiz, J. and B. M. Ebrahimi, "Mixed fault diagnosis in three-phase squirrel-cage induction motor using analysis of air-gap magnetic field," *Progress In Electromagnetics Research*, Vol. 64, 239–255, 2006.
14. Vaseghi, B., N. Takorabet, and F. Meibody-Tabar, "Transient finite element analysis of induction machines with stator winding turn fault," *Progress In Electromagnetics Research*, Vol. 95, 1–18, 2009.
15. Faiz, J., B. M. Ebrahimi, and M. B. B. Sharifian, "Time stepping finite element analysis of broken bars fault in a three-phase squirrel-cage induction motor," *Progress In Electromagnetics Research*, Vol. 68, 53–70, 2007.
16. Touati, S., R. Ibtiouen, O. Touhami, and A. Djerdir, "Experimental investigation and optimization of permanent magnet motor based on coupling boundary element method with permeances network," *Progress In Electromagnetics Research*, Vol. 111, 71–90, 2011.
17. Lecointe, J.-P., B. Cassoret, and J. Brudny, "Distinction of toothing and saturation effects on magnetic noise of induction motors," *Progress In Electromagnetics Research*, Vol. 112, 125–137, 2011.
18. Mahmoudi, A., N. Rahim, and H. Ping, "Axial-flux permanent-magnet motor design for electric vehicle direct drive using sizing equation and finite element analysis," *Progress In Electromagnetics Research*, 122, 467–469, 2012.